

# A statistical approach to crowdsourced smartphone-based earthquake early warning systems

Francesco Finazzi · Alessandro Fassò

Received: date / Accepted: date

**Abstract** The Earthquake Network research project implements a crowdsourced earthquake early warning system based on smartphones. Smartphones, which are made available by the global population, exploit the Internet connection to report a signal to a central server every time a vibration is detected by the on-board accelerometer sensor.

This paper introduces a statistical approach for the detection of earthquakes from the data coming from the network of smartphones. The approach allows to handle a dynamic network in which the number of active nodes constantly changes and where nodes are heterogeneous in terms of sensor sensibility and transmission delay. Additionally, the approach allows to keep the probability of false alarm under control.

The statistical approach is applied to the data collected by three subnetworks related to the cities of Santiago de Chile, Iquique (Chile) and Kathmandu (Nepal). The detection capabilities of the approach are discussed in terms of earthquake magnitude and detection delay.

A simulation study is carried out in order to link the probability of detection and the detection delay to the behaviour of the network under an earthquake event.

**Keywords** Sensor networks · Stochastic Processes · Maximum Likelihood · Android

Francesco Finazzi  
Dept. of Management, Economics and Quantitative Methods, University of Bergamo  
via dei Caniana, 2 - 24127 Bergamo, Italy  
E-mail: francesco.finazzi@unibg.it

Alessandro Fassò  
Dept. of Management, Information and Production Engineering, University of Bergamo  
via Marconi, 5 - 24044 Dalmine, Italy E-mail: alessandro.fasso@unibg.it

## 1 Introduction

Earthquake early warning (EEW) systems are intended to alert population and first responder agencies when harmful earthquakes strike. These systems are typically based on networks of stations with sensors measuring seismic and GPS data in real time [9, 10]. When an earthquake strikes, the earthquake is detected within few seconds and the population is possibly notified before strong shaking is experienced.

EEW systems require hundreds of stations located nearby known fault traces. Construction, maintenance and operation costs can be in the millions of dollars [10]. Recently, crowdsourced systems based on network of smartphones have been exploited in different social and environmental applications [13]. In [16], the temperature measured by smartphones is used to study the so called urban heat island effect while the iSPEX project [18] aims at measuring some properties of atmospheric aerosols using spectropolarimeters mounted on a large number of smartphones.

Crowdsourced EEW systems based on smartphones have been theorized and their detection capabilities have been studied mainly through simulations [15]. Accelerometric and GPS sensors on-board off-the-shelf smartphones can be exploited to detect ground shaking and thus possible earthquakes. Smartphone-based EEW systems are possibly based on thousands/millions of smartphones with zero construction costs and near zero maintenance costs. Classic EEW and smartphone-based EEW systems, however, differ in many respects. First of all, low-cost sensors on-board smartphones are not specifically designed to detect earthquakes. Secondly, a crowdsourced EEW system is based on heterogeneous smartphones from different vendors and thus on different sensors. Last and most importantly, smartphones of a crowdsourced EEW system are located where people are, partly reducing the benefits of the EEW system itself. Nonetheless, an earth-

quake detected by the smartphones of a city or town can be notified to the rest of the population not yet reached by the earthquake.

In this paper, we study the detection capabilities of the crowdsourced EEW system developed within the Earthquake Network project ([www.earthquakenetwork.it](http://www.earthquakenetwork.it)). The detection capabilities are evaluated in terms of detection rate and detection delay using both real data and simulated data.

The rest of the paper is organized as follows. Section 2 briefly introduces the Earthquake Network project while Section 3 details the statistical approach adopted to detect earthquakes from the data coming from the smartphone network. Section 4 introduces the data sets used to demonstrate the detection capabilities of the statistical approach, which is applied on Section 5. A simulation study on the detection delay is carried out in Section 6 and conclusions are given in Section 7.

## 2 The Earthquake Network project

Nowadays smartphones are equipped with accelerometric sensors that can be exploited to measure the ground motion induced by an earthquake [8, 6]. The Earthquake Network project aims at implementing and maintaining a global EEW system based on smartphone networks, with the smartphones voluntarily made available by the global population. The Earthquake Network EEW system detects earthquakes in real time and notifies the population as soon as possible, compatibly with the latencies of mobile telecommunications technologies. The project started at the beginning of 2013 and the system is currently based on a global network of around 70,000 smartphones.

The Earthquake Network project is similar in scope to the Quake Catcher Network (QCN) project [5] and the Community Seismic Network (CSN) monitoring system [4] though both QCN and CSN currently rely on Internet-connected computers with built-in or plugged-in accelerometric sensors. While the scope is similar, the inherent differences between computers and smartphones imply a different hardware and software architecture and a different data acquisition strategy. A key aspect of the Earthquake Network project is that smartphones have built-in accelerometric sensors while personal computers require an external device to be installed. It follows that smartphones are part of the EEW system by simply installing from the Internet the Earthquake Network smartphone application (<https://play.google.com/store/apps/details?id=com.finazzi.distquake>).

Although, for reasons of brevity, the hardware and software architecture of the Earthquake Network EEW system are not discussed in details this paper, the essential features of our EEW system are sketched here.

When the smartphone owner installs the Earthquake Network application, the smartphone becomes a node of the

EEW system. A smartphone enters the *active status* after that it has been connected to a source of power (to avoid battery drainage), that it has been recognized to be in a stationary condition (not in use and not exposed to systematic movements) and that a sensor calibration has been performed.

An active smartphone constantly monitors its acceleration and it sends an *active signal* to the server every 30 minutes. Active signals are used to describe the state of the network, in terms of number of active nodes and their spatial distribution.

When an active smartphone detects a vibration, it sends a *vibration signal* to the server with information on the geographic position of the smartphone (latitude and longitude). If the number of signals received is high with respect to the active smartphones for a certain area, the server issues an earthquake warning to the network.

This paper focuses on the detection algorithm implemented server-side. At the current stage of the project, epicenter and magnitude are not estimated and the earthquake is simply located at the centroid of the area where the earthquake is detected. Epicenter and magnitude estimation techniques for EEW systems are well studied in literature [12, 17] and their applicability to the Earthquake Network EEW system is still under evaluation.

## 3 Statistical EEW

This section introduces a strategy which aims at detecting an earthquake as soon as possible by the real-time analysis of the data collected by the network of smartphones and sent to the server.

In classic EEW systems, an earthquake warning can be issued when one or few seismometers in the network detect the first P-waves generated by the earthquake (see for instance 7). In the case of the Earthquake Network EEW system, it is observed that each smartphone in the network sends, on average, around 30 vibration signals per day not related to earthquakes. Indeed, though the application running on the smartphone filters some of these signals, many of them are not discriminable at the smartphone level and, henceforth, they are sent to the server. It follows that the server must be able to detect an earthquake by identifying vibration signals which are related to a real earthquake.

In the sequel, the term *false signal* will be used to denote a false vibration signal sent by a smartphone while the term *false alarm* will be used to denote a false earthquake warning issued by the detector. In order to keep the probability of false alarm under control, a statistical strategy is adopted and a statistical algorithm used for detection will be called here a *detector*.

Since the network of smartphones do not share a common clock, the server time is considered as reference. Trans-

mission delays are not measured nor estimated and they are assumed to be negligible with respect to the detection problem. Moreover, a fixed spatial area is considered, such as a city or a small region.

### 3.1 Stochastic modeling of vibration signals

Arrival times of the vibration signals are modeled through a stochastic point process under the hypothesis of no earthquake and deviation from this hypothesis is tested each time a vibration signal reaches the server.

Let  $\{N(t), t > t_0\}$  be the stochastic point process giving the probabilistic framework for the observed vibration signals coming from the network at arrival times  $t_1 < \dots < t_T$ . In particular, under the no earthquake hypothesis,  $N(t)$  is assumed to be a Poisson process with conditional intensity function

$$\lambda^0(t) = \lambda^0(t, \mathbf{x}_t)$$

where  $\mathbf{x}_t$  is a vector of covariates. According to standard notation, the number of vibration signals in the interval  $I = (a, b]$  is denoted by  $N(I)$  and is known to have Poisson distribution with expectation

$$E[N(I) | \mathbf{x}_t] = \Lambda(I | \mathbf{x}_t) = \int_I \lambda^0(t) dt.$$

Notice that, despite the no earthquake hypothesis,  $\lambda$  may show relevant variations due to day/night behavior and trends in the network size driven by external factors. In particular the number of active smartphones at time  $t$  is a relevant quantity. Although this quantity is difficult to be known exactly in real time, a proxy given by the number of active signals in the last 30 minutes, say  $v_t$ , is routinely available on the server with cheap computational cost and, with abuse of language, it will be called number of active smartphones in the sequel. As a result a Poissonian GLM is used with

$$\lambda^0(t) = \exp(\beta_0 + \beta_1 v_t) \quad (1)$$

where  $\beta = (\beta_0, \beta_1)'$  is the parameter vector to be estimated on historical no earthquake data.

### 3.2 Continuous time detectors

As the earthquake waves propagate at a given speed from the epicenter, the earthquake is not instantly felt by all the active smartphones in the network. Additionally, random transmission delays are possible. For these reasons, the vibration signals in the interval  $I_\varepsilon^t = (t - \varepsilon, t]$ , for some  $\varepsilon > 0$ , are considered as information related to the same earthquake and their number is denoted by  $N_\varepsilon^t = N(I_\varepsilon^t)$ .

Since  $\varepsilon$  is relatively small (e.g. 30 s) it is not easy to use standard change point detection techniques [1] which

are tailored for permanent changes and asymptotic theory. Additionally, control chart techniques based on the Poisson distribution [2, 11, 14] are not useful here as  $N_\varepsilon^t$  is computed at each vibration signal arrival and, especially under an earthquake event, the  $N_\varepsilon^t$  are not i.i.d.

Hence two likelihood approaches based on the generalized likelihood ratio (GLR) statistic (see for instance [3]) and on the efficient score, respectively, are considered in the sequel. Although the first one will result in a detector which is too slow to be computed in real time, it is presented here because it is a useful introduction to the score detector.

We begin with the well known log-likelihood of the signals in the interval  $I_\varepsilon^t$  [19] which is given by

$$\log L(\lambda | t, \varepsilon) = \sum_{t_j \in I_\varepsilon^t} \log \lambda(t_j) - \Lambda(I_\varepsilon^t) \quad (2)$$

where  $t_j$  are the arrival times of the vibration signals in  $I_\varepsilon^t$ .

Now suppose that, under a seismic event, the process intensity has a peak given by

$$\lambda(t) = \lambda^0(t) + \frac{\Delta}{\varepsilon}$$

with  $\Delta > 0$  for  $t \in I_\varepsilon^t$  and  $\Delta = 0$  otherwise. The log-likelihood in equation (2) has the following form

$$\log L(\Delta) = \sum_{t_j \in I_\varepsilon^t} \log \left( \lambda^0(t_j) + \frac{\Delta}{\varepsilon} \right) - \Lambda^0(I_\varepsilon^t) - \Delta.$$

For fixed  $\varepsilon$ , the GLR statistic is given by

$$\begin{aligned} GLR(\varepsilon, t) &= \log \frac{L(\hat{\Delta}_\varepsilon^t)}{L(0)} \\ &= \sum_{t_j \in I_\varepsilon^t} \log \left( 1 + \frac{\hat{\Delta}_\varepsilon^t}{\varepsilon \lambda^0(t_j)} \right) - \hat{\Delta}_\varepsilon^t \end{aligned}$$

where

$$\hat{\Delta}_\varepsilon^t = \max \left( 0, \arg \max_{\Delta} L(\Delta) \right)$$

and where  $\arg \max_{\Delta} L(\Delta)$  is given by the solution of the following likelihood equation

$$\sum_{t_j \in I_\varepsilon^t} \frac{1}{\varepsilon \lambda^0(t_j) + \Delta} - 1 = 0.$$

This can be solved numerically using as initial value the method of moment estimate of  $\Delta$ , which is easily seen to be given by  $\tilde{\Delta} = N_\varepsilon^t - \Lambda^0(I_\varepsilon^t)$ . The above GLR depends on the detection interval size  $\varepsilon$  which is arbitrary. Hence, extending [1], a GLR detector gives an earthquake warning if

$$\sup_{\varepsilon > 0} GLR(\varepsilon, t) > h$$

for some threshold  $h$  and  $\lambda^0(t)$  is computed using equation (1).

The second likelihood approach is based on the efficient score which is given by

$$S(\varepsilon, t) = \left. \frac{\partial}{\partial \Delta} \log L(\Delta) \right|_{\Delta=0} = \sum_{t_j \in I_\varepsilon^t} \frac{1}{\varepsilon \lambda^0(t_j)} - 1$$

and the score detector gives an earthquake warning if

$$\sup_{\varepsilon > 0} S(\varepsilon, t) > h \quad (3)$$

for some threshold  $h$ .

For small  $\varepsilon$ , the intensity  $\lambda^0$  can be assumed approximately constant in  $I_\varepsilon^t$  and considering the fast dynamics of the earthquake, an approximate score detector is given by

$$S(\varepsilon, t) \cong \frac{N_\varepsilon^t}{\varepsilon \lambda^0(t)} - 1 > h \quad (4)$$

for some  $h$ , which is quite faster to be computed with respect to detector given by (3).

### 3.3 Threshold modeling

A critical aspect for the detectors defined above is the choice of the threshold  $h$ . Indeed, there is a trade-off between the probability of false alarm  $\alpha = P(S(\varepsilon, t) > h \mid \Delta = 0)$  and the probability of missed detection of an earthquake, namely  $P(S(\varepsilon, t) < h \mid \Delta = \Delta^*)$  for a certain  $\Delta^* > 0$ . A low value of  $h$  implies a higher detection probability but also a higher probability of false alarm. Additionally, a higher value of  $h$  implies a higher detection delay when a real earthquake is striking. Since an uncontrolled and possibly large number of false alarms makes the warning system ineffective and at hand lead people to abandon the network, we give higher priority at controlling the probability of false alarm  $\alpha$ .

It is than a natural choice to take  $h$  as a quantile of the distribution of the score  $S(\varepsilon, t)$  under the null hypothesis of no earthquake, corresponding to a very small  $\alpha$  or a very large time between false alarms which is approximately  $1/\alpha$ . Unfortunately the exact distribution of  $S(\varepsilon, t)$  is not readily available and the asymptotic normality of the score statistic cannot be used here because  $\varepsilon$  is small and the Gaussian approximation is not satisfactory, especially in the far right tail of the detector distribution. The tail distribution is then estimated directly on data, thus giving a robust approach against violation of the parametric assumptions of the previous section.

To do this, firstly, a long sample is extracted from the dataset under no earthquake conditions. Secondly, the right tail of the empirical distribution above the  $p_0$  quantile (say  $p_0 = 0.99$ ) is considered and modeled through a generalized Pareto distribution. In order to have an average of one false

alarms over the period  $\Delta T$  (e.g. one false alarm per year), we set  $\alpha = \overline{\Delta t} / \Delta T$  where  $\overline{\Delta t}$  is the observed mean time between (false) vibration signals. Finally,  $h$  is given by the  $p_1$  quantile of the generalized Pareto distribution, with  $p_1 = 1 - \frac{\alpha}{1-p_0}$ ,

## 4 Earthquake data

The Earthquake Network project started on January 1st, 2013. Since then, the Android application has been downloaded more than 650,000 times and the network has grown up to around 70,000 users globally. As participation to the network is voluntary, the number of users in the network changes continuously as well as their spatial distribution. In general, strong earthquakes felt by the population induce a large number of downloads and the spontaneous growth of new subnetworks. In many cases, subnetworks coincide with cities where users are clustered. Subnetworks are characterized by their own life cycle and they may disappear if users lose interest.

This paper considers the three subnetworks of Santiago de Chile (Chile), Iquique (Chile) and Kathmandu (Nepal), in year 2015 as specified in Table 1. The subnetworks of Santiago de Chile and Iquique are quite stable in time, with the former bigger than the latter. Conversely, the Kathmandu subnetwork has grown rapidly after the 7.8 magnitude earthquake that hit Nepal on April 25, 2015.

Figure 1 shows the Santiago de Chile subnetwork in the early morning of a working day. Note that the spatial pattern of the smartphones reflects the population distribution within the subnetwork. Also note that only a fraction of the smartphones is active (green dots).

In order to demonstrate the functioning of the detector  $S(\varepsilon, t)$  above introduced, data coming from each subnetwork have been collected over the time frame reported in Table 1. Statistics related to the active smartphones, given in the same table, refer to the number of smartphones which are active at any given time during the day. This number is significantly lower than the number of users which take part in the subnetwork as, at any given time, a fraction of smartphones is switched off and another fraction is not active. The number of active smartphones largely changes during the day and it is usually higher at night (when people charge their smartphones) and lower at daytime. A weekend effect is also observed, with the average number of active smartphone which is lower during the weekend.

## 5 Data analysis

Data collected from each subnetwork consist in the time-ordered list,  $\mathcal{L}$  say, of the timing of each vibration signal received by the server, together with smartphone georefer-

**Table 1** Subnetwork details and statistics of active smartphones. Symbols  $\tilde{v}_5$ ,  $\bar{v}$  and  $\tilde{v}_{95}$  denote, respectively, 5th percentile, average and 95th percentile of the number of active smartphones.

Subnetwork	Diameter	Population	Time frame	Active smartphones		
				$\tilde{v}_5$	$\bar{v}$	$\tilde{v}_{95}$
Santiago (Chile)	40 km	6,300,000	Jan 7, 2015 - Apr 9, 2015	51	183	416
Iquique (Chile)	15 km	182,000	Jan 7, 2015 - Apr 9, 2015	29	78	165
Kathmandu (Nepal)	30 km	1,000,000	Apr 25, 2015 - May 15, 2015	15	38	70

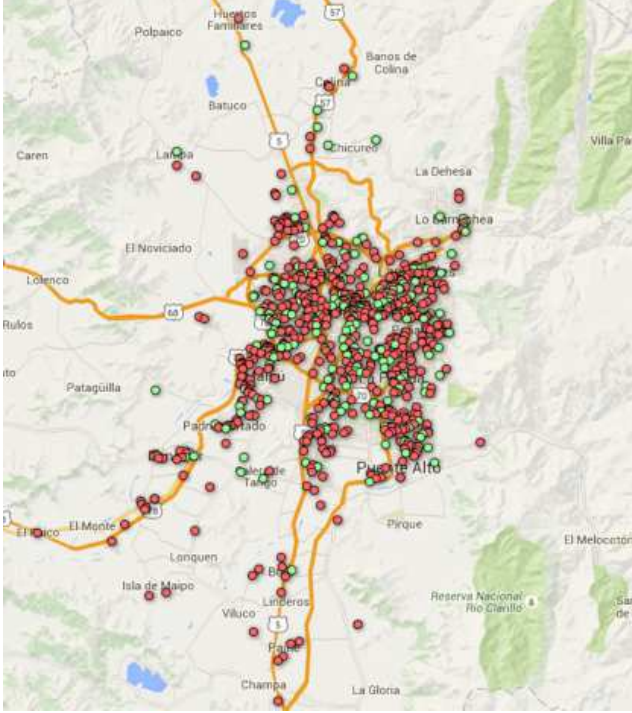


**Fig. 1** Santiago de Chile subnetwork at 6:30 (local time) of a typical working day. Green dots are the active smartphone while the red dots are smartphone connected to Internet but not active at that time.

encing (latitude and longitude) and the estimated number of active smartphones  $v_i$  in the subnetwork.

As the statistical distribution of the detector  $S(\varepsilon, t)$  is derived under the hypothesis of no earthquake, it is necessary to obtain the list  $\mathcal{L}^0$  of all the vibration signals not induced by a real earthquake (false signals). This is done considering the catalog of the European Mediterranean Seismological Centre (EMSC) which provides information on the earthquakes detected globally. Earthquakes occurred within a radius of 1000 km from each subnetwork, and likely felt, are firstly identified and then used to derive  $\mathcal{L}^0$  removing from  $\mathcal{L}$  all the signals received from the beginning of each earthquake up to 5 minutes later. Indeed, even if an earthquake duration is in the range of seconds, after a seismic event, the network may experience a sudden transient related to phone lines crowding, switch off and other outlying behaviors.

The choice of the window size  $\varepsilon$  may influence the detection probability and the probability of false alarm. In this

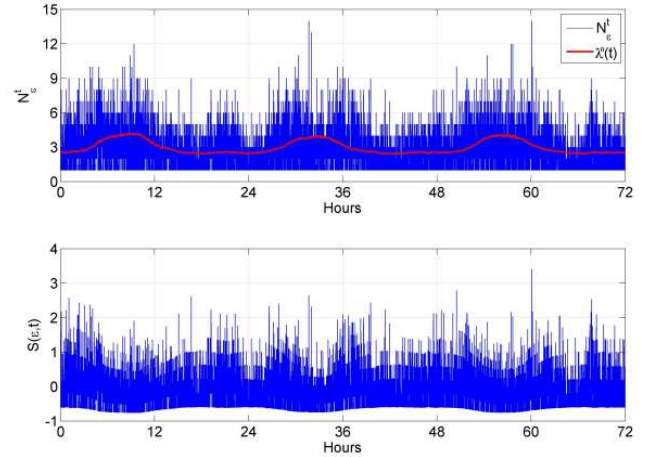


**Fig. 2** Graphs of  $N_\varepsilon^t$ ,  $\lambda^0(t)$  and  $S(\varepsilon, t)$  evaluated for the Santiago de Chile subnetwork over 3 days starting from February 25, 2015 00:00 (UTC).

work  $\varepsilon = 30$  s is used and its choice is justified in Section 6 by simulation results.

## 5.1 Parameter estimation

The vibration signals in the list  $\mathcal{L}^0$  are used to estimate the parameters of  $\lambda^0(t) = \exp(\beta_0 + \beta_1 v_i)$  which is needed to compute  $S(\varepsilon, t)$  as in equation (4). Table 2 reports the estimates of  $\beta_0$  and  $\beta_1$ , which are obtained by the maximum likelihood method and have standard deviations smaller than  $9 \times 10^{-3}$  and  $2 \times 10^{-4}$ , respectively, for all the subnetworks.

Considering  $\varepsilon = 30$  s, equation (4) is used to compute  $S(\varepsilon, t)$  for each signal in  $\mathcal{L}^0$ . As an example, Figure 2 shows the graphs of  $N_\varepsilon^t$ ,  $\lambda^0(t)$  and  $S(\varepsilon, t)$  for the Santiago de Chile subnetwork over a period of 3 days and for around 18,600 vibration signals received. Note that  $N_\varepsilon^t$  reflects the daily cycle of the number of active smartphones and that the server received up to 14 vibration signals in less than 30 s even in the absence of earthquakes. This shows that each smartphone, taken individually, is not a reliable seismometer and a statistical approach, which is able to discriminate real earthquakes, is useful.

Following the procedure detailed in Section 3.3 and considering  $p_0 = 0.99$ , the empirical distribution of  $S(\varepsilon, t)$  is analysed to derive a threshold  $h$  corresponding to a mean

**Table 2** GLM parameter and threshold estimation. Legend:  $|\mathcal{L}^0|$ : number of false signals observed over the time frame specified in Table 1;  $\hat{\beta}_0$  and  $\hat{\beta}_1$ : estimated parameters of the GLM;  $\overline{\Delta t}$  (s): average inter-arrival time;  $p_1$ : percentile of the Pareto distribution;  $h$ : estimated threshold.

Subnetwork	$ \mathcal{L}^0 $	GLM		Threshold estimation		
		$\hat{\beta}_0$	$\hat{\beta}_1$	$\overline{\Delta t}$ (s)	$p_1$	$h$
Santiago de Chile	442,000	0.7694	0.0016	18.0	0.99994	6.42
Iquique	208,000	0.4111	0.0027	38.2	0.99988	4.21
Kathmandu	19,400	0.1190	0.0068	88.6	0.99972	4.16

time between false alarms of approximately one year. Table 2 reports the intermediate results and the estimated  $h$ .

## 5.2 Earthquake detection

With the threshold  $h$  available, the detector  $S(\varepsilon, t)$  is used to detect an earthquake every time  $S(\varepsilon, t)$  exceeds  $h$ . Typically, the detector works in an on-line manner, that is,  $S(\varepsilon, t)$  is computed every time the server receives a vibration signal and an earthquake warning is issued when  $S(\varepsilon, t) > h$ . Here, the detector is applied off-line to the list  $\mathcal{L}$  in order to show its detection capabilities on past earthquakes.

Note that the detector is not guaranteed to detect all the earthquakes that was felt in a given subnetwork. If the number of active smartphones is too low and/or the earthquake is very mild, then the earthquake may not be recognized from the “background noise”.

Tables 3 reports, for each subnetwork, the information on the earthquakes which are detected over the time frames specified in Table 1. Earthquake time, latitude, longitude, depth and magnitude are obtained from the above mentioned EMSC catalog while the distance is computed from the epicenter to the centre of the subnetwork. The detection time  $t^*$  refers to the time at which  $S(\varepsilon, t)$  exceeds  $h$  while the delay is computed as the difference between  $t^*$  and the first vibration signal received by the server and related to the earthquake. The table also reports the number of active smartphones at  $t^*$ , the number of vibration signals induced by the earthquake and the fraction of active smartphones that sent a vibration signal.

As different earthquakes are characterized by different parameters (mainly magnitude, depth and distance) it is not easy to derive final conclusions on the behaviour of the subnetworks under an earthquake event. Nonetheless, some general comments can be made. First of all, mild earthquakes (say below magnitude 4) are not detected. The accelerometer on-board the smartphone may not be sensible enough to detect a vibration or the earthquake is detected by a very small number of smartphones. Secondly, the fraction of active smartphones reporting a vibration signal is, on average, 0.31 and it is rarely higher even in the case of strong earthquakes. This is because, by chance, smartphones may be located over soft and vibration absorbing surfaces which reduce the acceleration induced by an earthquake, or the In-

ternet connection may not be available at the time the earthquake is felt. Finally, the detection delay (which does not include the delay due to the distance from the epicenter) ranges from 2 to 17 s. This delay is influenced by the temporal spread of the vibration signals which are sent to the server; the lower the spread the lower the detection delay.

Note that two of the earthquakes detected by the subnetworks are actually false alarms. False alarms are likely related to the behaviour of the users with the smartphone application installed. Indeed, the application allows to receive many kind of notifications (e.g. the notifications related to the earthquakes detected by the national and international seismic networks). Since these notifications are received by many users within a short time frame, the same users may induce multiple vibrations (for instance by picking up the smartphone) which are sent to the server and which are identified as an earthquake. This problem will be solved with future released of the smartphone application, allowing to reduce the occurrence of “clusters” of false vibration signal, to lower the threshold  $h$  and thus to lower the detection delay.

As an example, Figure 3 shows the behavior of  $S(\varepsilon, t)$  for an earthquake that affected the subnetwork of Santiago de Chile. The earthquake struck on February 24, 2015 at 05:14:02 UTC, with moment magnitude 4.9 and with epicenter 136 km from Santiago de Chile (see Table 3). Each bar in the graph of Figure 3 represents the value of  $S(\varepsilon, t)$  evaluated at the arrival of a vibration signal. Before the earthquake, the arrivals are sparse in time and  $S(\varepsilon, t)$  is low. When the subnetwork senses the earthquake, the arrivals are close in time and  $S(\varepsilon, t)$  exceeds the threshold  $h$  after few seconds. The warning was issued 43 seconds after the earthquake, though this delay includes the time required to the earthquake waves to cover the distance between the epicenter and Santiago de Chile.

## 5.3 Warning time

To be effective, an EEW system should alert the population (or part of it) many seconds in advance in order to allow people to take cover. The image of Figure 4 depicts the warning times related to the magnitude 7.3 earthquake event of May 12, 2015 with epicenter in Nepal. More than 150 people were killed by the earthquake and more than 3,200 people were injured.

**Table 3** Real earthquakes and false alarms signaled by  $S(\epsilon, t)$ . Legend: Earthquake time: UTC of the earthquake from EMSC catalog; Lat., Lon.: epicenter location; Mag.: earthquake magnitude; Dist.: distance between epicenter and subnetwork centre; Detection time: UTC of detection; Delay: detection delay wrt first vibration signal related to the earthquake;  $v_t$ : number of active smartphones at detection time;  $\tilde{N}$ : total number of vibration signals received by the server during the earthquake;  $f$ : fraction of active smartphones that reported the earthquake.

Santiago de Chile subnetwork										
Earthquake time	Lat.	Lon.	Depth	Mag.	Dist.	Detection time	Delay	$v_t$	$\tilde{N}$	$f$
15/01/2015 05:19:45	-33.61°	-71.22°	80 km	<i>mb</i> 4.6	56 km	15/01/2015 05:20:09	6 s	147	73	0.50
25/01/2015 08:47:04	-34.72°	-71.67°	40 km	<i>mb</i> 4.7	168 km	25/01/2015 08:47:50	11 s	151	50	0.33
False alarm										
17/02/2015 14:35:55	-32.33°	-70.74°	94 km	<i>Mw</i> 5.4	127 km	17/02/2015 14:36:37	17 s	71	24	0.34
24/02/2015 05:14:02	-32.63°	-71.71°	60 km	<i>mb</i> 4.9	136 km	24/02/2015 05:14:45	10 s	303	101	0.33
01/04/2015 15:54:14	-33.74°	-71.02°	67 km	<i>ML</i> 4.0	46 km	01/04/2015 15:54:43	12 s	93	23	0.25
Iquique subnetwork										
Earthquake time	Lat.	Lon.	Depth	Mag.	Dist.	Detection time	Delay	$v_t$	$\tilde{N}$	$f$
09/01/2015 11:48:28	-20.43°	-68.94°	109 km	<i>Mw</i> 4.8	128 km	09/01/2015 11:49:12	7 s	70	24	0.34
24/02/2015 05:13:50	-22.70°	-66.68°	182 km	<i>mb</i> 5.3	452 km	24/02/2015 05:14:51	7 s	119	12	0.10
03/03/2015 12:45:18	-20.39°	-69.03°	104 km	<i>Mw</i> 5.1	118 km	03/03/2015 12:45:49	7 s	47	9	0.19
09/03/2015 03:22:20	-19.70°	-69.33°	91 km	<i>mb</i> 4.7	102 km	09/03/2015 03:22:59	15 s	102	17	0.17
False alarm										
23/03/2015 04:51:38	-18.46°	-69.17°	132 km	<i>Mw</i> 6.4	220 km	23/03/2015 04:52:16	3 s	124	51	0.41
Kathmandu subnetwork										
Earthquake time	Lat.	Lon.	Depth	Mag.	Dist.	Detection time	Delay	$v_t$	$\tilde{N}$	$f$
12/05/2015 07:05:19	27.89	86.17	10 km	7.3 <i>Mw</i>	85 km	12/05/2015 07:05:42	4 s	32	11	0.34
12/05/2015 20:22:15	27.57	85.06	10 km	4.5 <i>mb</i>	30 km	12/05/2015 20:22:21	2 s	42	23	0.55
15/05/2015 01:42:43	28.09	84.9	10 km	4.9 <i>mb</i>	61 km	15/05/2015 01:43:06	5 s	87	14	0.16

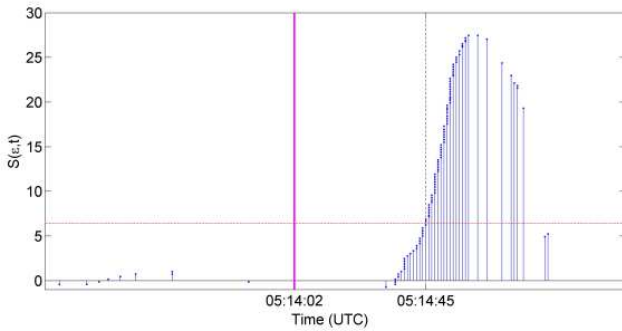


**Fig. 3** Graph of  $S(\epsilon, t)$  before and after the earthquake detected by the Santiago de Chile subnetwork on February 24, 2015 05:14:55 (UTC). Legend: vertical bars: value of  $S(\epsilon, t)$  computed at each vibration signal; vertical solid line: time of the earthquake at the epicenter; vertical dashed line: detection time; horizontal dashed line: threshold  $h$ .

The earthquake was detected by the Kathmandu subnetwork with a delay of 4 s from the first vibration signal received by the server. It is assumed here that the first smartphone detected the earthquake 1.5 seconds from the beginning of the ground shaking and that the transmission delay from the smartphone to the server was 0.5 s. Moreover, it is assumed that the server took 0.5 s to notify the users with the Earthquake Network application installed, bringing the total delay to 6.5 s. From the scientific data of the EMSC catalog, the speed of the earthquake waves is estimated to be  $0.0715^\circ/s$  and it is assumed to be isotropic. Each circle in the image of Figure 4 represents a warning time. The population inside the 0 s circle received the earthquake warning

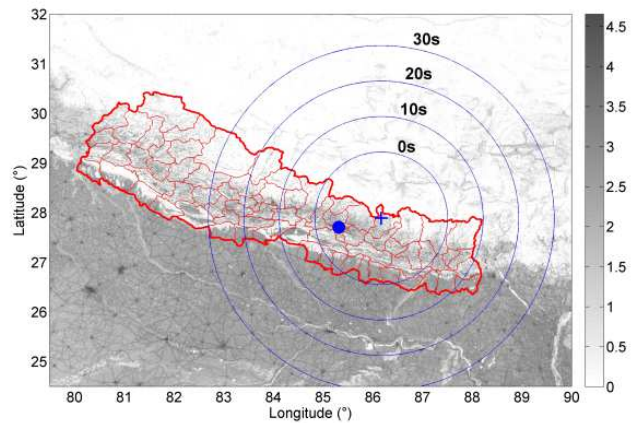


**Fig. 4** Forewarning times for the magnitude 7.3 earthquake of May 12, 2015 in Nepal. Legend: cross: earthquake epicenter; filled dot: Kathmandu subnetwork; circles: forewarning radius of 0, 10, 20 and 30 seconds; colormap:  $\log_{10}$ -population.

after having experienced the earthquake while the population outside received the warning in advance, with a warning time proportional to the distance between each person and the epicenter. Figure 4 suggests that the EEW system is more effective when the earthquake is detected near the epicenter, in which case it is possible to notify in advance a higher population fraction.

## 6 Detection delay simulation

A set of realistic simulations is carried out to understand the performances of the Earthquake Network EEW system in terms of detection probability and detection delay. The focus is on the network behavior under a seismic event, rather than the physical dynamics of the seismic event itself. In particular it is implicitly assumed that the seismic intensity is constant over the area considered.

The main simulation parameter are the report fraction  $\phi$  and the report spread  $\sigma$ . Indeed, when an earthquake is assumed to hit the geographic area of the subnetwork under study,  $\phi$  is the fraction of active smartphones that reports a vibration signal. Since strong earthquakes are felt by a large fraction of smartphones,  $\phi$  essentially describes the earthquake intensity. On the other side,  $\sigma$  is the time distance between the first and the last vibration signals received by the server. It describes the (random) delays that prevent the vibration signals to be notified to the server instantaneously.

Simulations are implemented considering the data of the Santiago de Chile subnetwork, and the time frame of Table 1 with the real earthquake events filtered out. For each combination of report fraction and report spread of Table 4, 1,000 earthquakes are simulated as follows. Firstly, an earthquake time  $\tau$  is randomly extracted over the range of the time frame. Secondly, the corresponding number of active smartphones  $v_\tau$  is used to simulate  $v_\tau \times \phi$  vibration signals, randomly located in the interval  $(\tau, \tau + \sigma)$ . The detector  $S(\varepsilon, t)$  is then applied and, in the case of detection, the detection delay  $t^* - \tau$  is evaluated, with  $t^*$  the detection time.

Table 4 shows the detection fraction which is an estimate of the detection probability. It is possible to note that the detection fraction is influenced by the report fraction while the report spread has no effect. In particular, when  $\phi > 0.25$ , the earthquake is detected with about 90% probability while  $\phi > 0.55$  guarantees almost sure detection.

Table 5 reports, instead, the average detection delay which is influenced by both  $\phi$  and  $\sigma$ . As expected, the lower  $\phi$  the lower the detection delay, while a lower  $\phi$  implies a higher delay.

Note that the delays reported in Table 5 are averages over 1,000 simulations. The delay related to a specific earthquake is also a function of the number of active smartphones. For instance, the graph of Figure 5 shows the detection delays for 1,000 simulations with  $\phi = 0.5$  and  $\sigma = 10$  s. The detection delay can be as high as 10 s when the number of active smartphones is lower than 50, while a number of active smartphones higher than 300 implies a delay between one and two seconds.

**Table 4** Detection fraction (in percentage) of the detector  $S(\varepsilon, t)$ ,  $\varepsilon = 30$  s, for 1,000 simulated earthquakes with respect to the report fraction  $\phi$  and the report spread  $\sigma$  (in seconds).

	$\sigma$						
	2	3	5	10	15	20	25
0.01	0.0	0.0	0.0	0.0	0.0	0.0	0.0
0.05	3.4	4.3	4.6	5.1	6.2	4.8	5.1
0.10	34.8	39.3	40.2	41.6	39.3	40.3	41.6
0.15	67.3	67.1	68.5	68.2	69.4	68.1	68.6
0.20	80.1	78.9	81.6	83.5	81.8	82.6	82.1
0.25	90.9	90.8	90.4	90.1	90.2	90.5	89.6
0.30	94.1	94.5	95.1	95.3	93.1	94.2	93.1
0.35	96.3	97.2	97.1	96.7	97.0	97.0	97.1
0.40	99.2	98.7	98.6	98.5	98.4	99.1	98.8
0.45	99.6	99.6	99.9	99.6	99.6	99.8	99.1
0.50	99.6	99.9	100.0	100.0	99.9	99.9	99.8
0.55	100.0	100.0	100.0	100.0	99.9	100.0	100.0
0.60	100.0	100.0	100.0	100.0	100.0	100.0	100.0
0.65	100.0	100.0	100.0	100.0	100.0	100.0	100.0
0.70	100.0	100.0	100.0	100.0	100.0	100.0	100.0
0.75	100.0	100.0	100.0	100.0	100.0	100.0	100.0
0.80	100.0	100.0	100.0	100.0	100.0	100.0	100.0

**Table 5** Average detection delay (in seconds) of the detector  $S(\varepsilon, t)$ ,  $\varepsilon = 30$  s, for 1,000 simulated earthquakes with respect to the report fraction  $\phi$  and the report spread  $\sigma$  (in seconds).

	$\sigma$						
	2	3	5	10	15	20	25
0.01	—	—	—	—	—	—	—
0.05	1.78	3.08	4.96	11.18	16.91	19.32	24.04
0.10	1.38	2.14	3.48	7.26	11.12	14.18	17.50
0.15	1.24	1.85	3.20	6.61	9.90	12.61	15.73
0.20	1.09	1.62	2.79	5.57	8.38	10.86	13.59
0.25	0.98	1.44	2.35	4.88	7.09	9.56	11.77
0.30	0.87	1.29	2.14	4.19	6.42	8.49	10.53
0.35	0.76	1.13	1.96	3.84	5.74	7.64	9.61
0.40	0.68	1.02	1.74	3.52	4.99	6.84	8.59
0.45	0.61	0.91	1.58	3.17	4.48	6.25	7.69
0.50	0.57	0.88	1.40	2.88	4.27	5.65	7.14
0.55	0.53	0.78	1.30	2.53	3.92	5.01	6.44
0.60	0.49	0.70	1.19	2.42	3.52	4.81	5.85
0.65	0.45	0.67	1.13	2.22	3.25	4.35	5.58
0.70	0.41	0.61	1.06	2.13	3.07	3.99	5.15
0.75	0.39	0.58	0.92	1.97	2.93	3.87	4.73
0.80	0.37	0.55	0.87	1.82	2.72	3.55	4.52

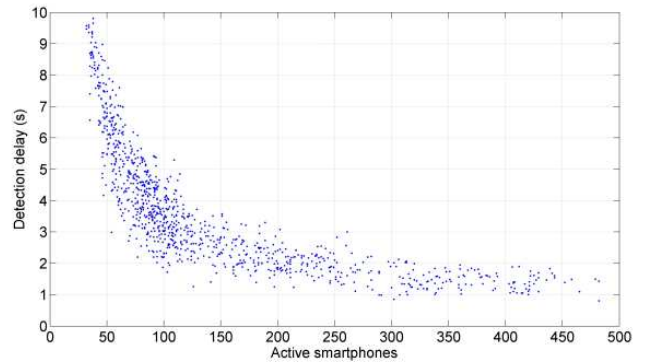


**Fig. 5** Detection delay with respect to the number of active smartphones  $v_\tau$ . Dots represent the detection delay for the 1,000 simulated earthquakes with report fraction  $\phi = 0.5$  and report spread  $\sigma = 10$  s.

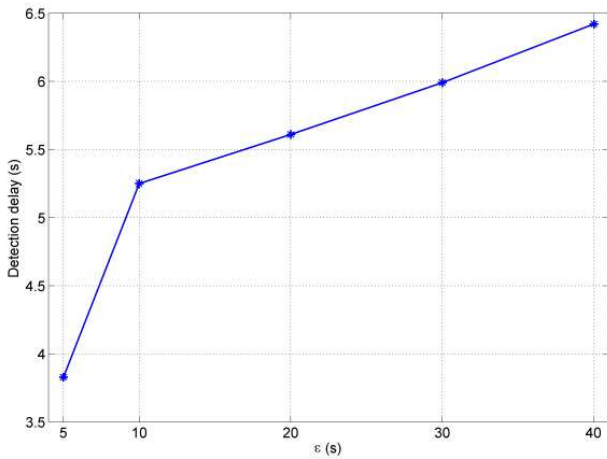


**Fig. 6** Detection delay vs window size  $\varepsilon$ . Delays are averaged over  $\phi$  and  $\sigma$  defined in Table 4.

### 6.1 Window size

As mentioned above, the choice of the window size  $\varepsilon$  has an impact on the behavior of the detector  $S(\varepsilon, t)$ . The choice of the window size has to take into account that, for smaller  $\varepsilon$  a shorter delay is expected but, if the number of active nodes  $v_i$  and/or the report fraction  $\phi$  are low, then a small  $\varepsilon$  entails a low detection fraction. That said, the false alarm probability  $\alpha$  is controlled for each  $\varepsilon$  since the threshold  $h$  is computed for fixed  $\varepsilon$ .

The simulations and statistics as in Tables 4 and 5 have been performed for  $\varepsilon = 5, 10, 20, 30, 40$  s. In Figure 6, the detection delay, averaged for  $\phi$  and  $\sigma$ , shows that increasing window size slows down the earthquake detection. On the other side, Figure 7 shows that for small  $\varepsilon$  the detection fraction is poor when the spread  $\sigma$  is large. For these reasons,  $\varepsilon = 30$  s used in this work is a good compromise between early detection, which applies to short spread events, and acceptable detection fraction for large spread.

## 7 Conclusions

EEW systems may save human lives in the case of destructive earthquake events. Especially in underdeveloped and developing countries, however, the proliferation of EEW systems may be dampened by the high installation and operating costs. In this paper it is shown that crowdsourced EEW systems based on smartphones can be used to detect earthquakes in quasi real-time and to alert the population through the very same devices, with zero installation costs and very low operating costs.

The problem of detecting earthquakes from the data sent by the smartphone network has been solved through a statistical approach which is able to handle a dynamic network and, more importantly, which allows to control the probabil-

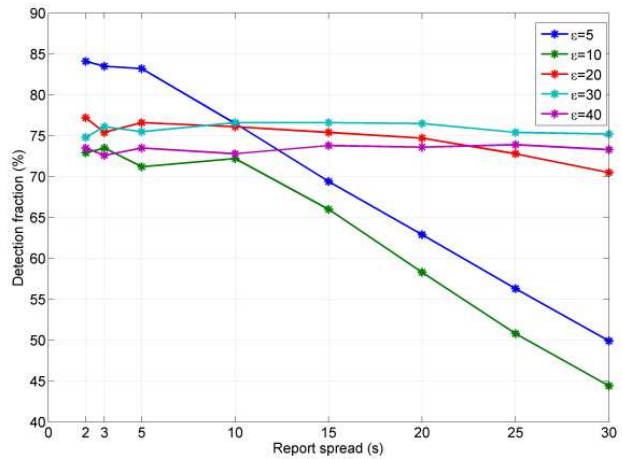


**Fig. 7** Detection fraction vs report spread  $\sigma$  for various window sizes  $\varepsilon$ . Detection fractions are averaged over  $\phi$  defined in Table 4.

ity of false alarms. The detection capabilities of the approach have been proven using real data collected by the crowdsourced EEW system of the Earthquake Network project. Considering three subnetworks of the smartphone network, the system was able to detect earthquakes down to magnitude 4 and with detection delays ranging from 2 to 17 seconds. The variability of the detection delay is quite high within and across subnetworks and it might be reduced considering the information on the spatial location of the smartphones. Indeed, the statistical approach developed in this paper does not fully exploit this information, which is only used to discriminate across subnetworks. Nonetheless, the approach has the advantage of being computationally fast and thus suitable for quasi real-time detection. Future works will try to extend the statistical approach in order to use the information on the smartphone location. This will allow to introduce a global detector which is not based on subnetworks and which is able to provide an estimate of the earthquake epicenter.

## References

1. Michèle Basseville, Igor V Nikiforov, et al. *Detection of abrupt changes: theory and application*, volume 104. Prentice Hall Englewood Cliffs, 1993.
2. Connie M Borror, Charles W Champ, and Steven E Rigdon. Poisson EWMA control charts. *Journal of Quality Technology*, 30(4):352–361, 1998.
3. Giovanna Capizzi and Guido Masarotto. Practical design of generalized likelihood ratio control charts for autocorrelated data. *Technometrics*, 50(3):357–370, 2008.
4. Robert W Clayton, Thomas Heaton, Mani Chandy, Andreas Krause, Monica Kohler, Julian Bunn, Richard Guy, Michael Olson, Mathew Faulkner, MingHei

- Cheng, et al. Community seismic network. *Annals of Geophysics*, 54(6), 2012.
5. Elizabeth S Cochran, Jesse F Lawrence, Carl Christensen, and Ravi S Jakka. The quake-catcher network: Citizen science expanding seismic horizons. *Seismological Research Letters*, 80(1):26–30, 2009.
  6. Elizabeth S Cochran, Jesse F Lawrence, Anna Kaiser, Bill Fry, Angela Chung, and Carl Christensen. Comparison between low-cost and traditional MEMS accelerometers: a case study from the M7.1 Darfield, New Zealand, aftershock deployment. *Annals of Geophysics*, 54(6), 2012.
  7. Georgia Cua, Michael Fischer, Thomas Heaton, and Stefan Wiemer. Real-time performance of the Virtual Seismologist earthquake early warning algorithm in southern California. *Seismological Research Letters*, 80(5):740–747, 2009.
  8. Antonino D’Alessandro and Giuseppe D’Anna. Suitability of low-cost three-axis MEMS accelerometers in strong-motion seismology: Tests on the LIS331DLH (iPhone) accelerometer. *Bulletin of the Seismological Society of America*, 103(5):2906–2913, 2013.
  9. Paolo Gasparini, Gaetano Manfredi, and Jochen Zschau. *Earthquake early warning systems*. Springer, 2007.
  10. Douglas D Given, Elizabeth S Cochran, Thomas Heaton, Egill Hauksson, Richard Allen, Peggy Hellweg, John Vidale, and Paul Bodin. Technical implementation plan for the ShakeAlert production system: an earthquake early warning system for the west coast of the united states. Technical report, US Geological Survey, 2014.
  11. B He, M Xie, TN Goh, and KL Tsui. On control charts based on the generalized Poisson model. *Quality Technology & Quantitative Management*, 3(4):383–400, 2006.
  12. M Lancieri and A Zollo. A bayesian approach to the real-time estimation of magnitude from the early P and S wave displacement peaks. *Journal of Geophysical Research: Solid Earth (1978–2012)*, 113(B12), 2008.
  13. Nicholas D Lane, Emiliano Miluzzo, Hong Lu, Daniel Peebles, Tanzeem Choudhury, and Andrew T Campbell. A survey of mobile phone sensing. *Communications Magazine, IEEE*, 48(9):140–150, 2010.
  14. Yajun Mei, Sung Won Han, and Kwok-Leung Tsui. Early detection of a change in Poisson rate after accounting for population size effects. *Statistica Sinica*, 21(2):597, 2011.
  15. Sarah E. Minson, Benjamin A. Brooks, Craig L. Glennie, Jessica R. Murray, John O. Langbein, Susan E. Owen, Thomas H. Heaton, Robert A. Iannucci, and Darren L. Hauser. Crowdsourced earthquake early warning. *Science Advances*, 1(3), 2015.
  16. Aart Overeem, JC R Robinson, Hidde Leijnse, Gert-Jan Steeneveld, BK P Horn, and Remko Uijlenhoet. Crowdsourcing urban air temperatures from smartphone battery temperatures. *Geophysical Research Letters*, 40(15):4081–4085, 2013.
  17. Claudio Satriano, Yih-Min Wu, Aldo Zollo, and Hiroo Kanamori. Earthquake early warning: Concepts, methods and physical grounds. *Soil Dynamics and Earthquake Engineering*, 31(2):106–118, 2011.
  18. Frans Snik, Jeroen HH Rietjens, Arnoud Apituley, Hester Volten, Bas Mijling, Antonio Di Noia, Stephanie Heikamp, Ritse C Heinsbroek, Otto P Hasekamp, J Martijn Smit, et al. Mapping atmospheric aerosols with a citizen science network of smartphone spectropolarimeters. *Geophysical Research Letters*, 41(20):7351–7358, 2014.
  19. Donald L Snyder and Michael I Miller. *Random point processes in time and space*. Springer Science & Business Media, 2012.